JACS Au
AN OPEN ACCESS JOURNAL OF THE AMERICAN CHEMICAL SOCIETY

pubs.acs.org/jacsau
Article

Manipulating the Interfacial Hydrophobic Microenvironment via Electrolyte Engineering Promotes Electrocatalytic Fatty Alcohol Oxidation Coupled with Hydrogen Production

Ruiqi Du, Zemao Chen, Shiyan Wang, Shumao Zeng, Rui Jia, Kaizheng Zhang, Diannan Lu, Haihui Wang,* and Yi Cheng*

Cite This: JACS Au 2025, 5, 1974−1982
Read Online
ACCESS | Metrics & More | Article Recommendations | Supporting Information

ABSTRACT: The selective oxidation of fatty alcohols to fatty acids represents a pivotal transformation in organic synthesis. Traditional methods often require harsh conditions and environmentally harmful oxidants or solvents. Electrocatalytic oxidation emerges as a promising green alternative, enabling mild oxidation in aqueous media and concurrent energy-efficient hydrogen production at the cathode. However, the poor solubility of fatty alcohols in water poses a significant challenge, reducing the reactant availability at the electrode surface, thereby hindering mass transfer and overall reaction rates. Herein, we develop an electrolyte engineering strategy that incorporates cetyltrimethylammonium hydroxide (CTAOH) as an additive. This strategy significantly enhances the oxidation current density of fatty alcohols as well as the production rate of fatty acids on a gold electrocatalyst. Through a mechanistic investigation combining experimental evidence from a quartz crystal microbalance (QCM) and in situ attenuated total reflectance surface-enhanced infrared spectroscopy (ATR-SEIRAS) with molecular dynamics (MD) simulations, we confirm that the preferential adsorption of CTAOH creates a hydrophobic interfacial microenvironment at the anode, promoting the enrichment of reactant at the electrode−electrolyte interface. This work highlights the significance of interfacial hydrophobicity modulation in boosting aqueous-phase electrocatalytic oxidation, paving the way for more efficient electrocatalytic transformations involving water-insoluble reactants.

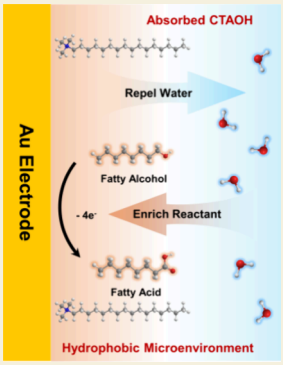

KEYWORDS: *electrocatalytic oxidation, fatty alcohol, electrolyte engineering, interfacial hydrophobicity*

1. INTRODUCTION

The selective oxidation of alcohols to carboxylic acids represents a pivotal class of organic synthetic transformations.[1−3] Fatty alcohols, specifically monohydric aliphatic alcohols with a alkyl chain length exceeding six, are precursors to fatty acids.[4] Particularly, fatty acids, regarded as valuable fine chemicals, find wide applications in industries such as cosmetics, plasticizers, and resins.[5,6] However, the inherent low reactivity of fatty alcohol molecules presents significant challenges in traditional oxidation methods.[7] Historically, these methods have relied on stoichiometric oxidants, many of which are toxic transition metal compounds.[8,9] Additionally, conventional approaches often necessitate high temperatures, elevated pressures, and the use of organic solvents, factors that contribute to environmental impacts and safety concerns.[10−12] Consequently, there is an urgent need for the development of greener and more sustainable protocols for the oxidation of fatty alcohols. Recently, electrocatalytic alcohol oxidation has emerged as a promising green oxidation method.[13,14] This method, powered by renewable energy, facilitates the oxidation of alcohols in aqueous media under mild conditions.[15,16] Furthermore, the synergy between electrocatalytic alcohol oxidation and the concurrent cathodic hydrogen evolution reaction significantly amplifies the overall efficiency of hydrogen production.[17,18] However, current research predominantly focuses on the electrocatalytic oxidation of short-chain alcohols, such as methanol and ethanol, which possess high solubility in an aqueous electrolyte. In contrast, the exploration of long-chain fatty alcohols, characterized by their hydrophobic nature, has been limited due to their low solubility in aqueous electrolytes.[8,19] This solubility limitation results in diminished reactant concentrations in the vicinity of the catalytic electrode, thereby hindering mass transfer and consequently impeding the efficiency of electrocatalytic reaction[20−22] (Figure 1a). Therefore, achieving efficient electrocatalytic oxidation of fatty alcohols remains a significant challenge.

Electrocatalytic reactions occur at the electrode−electrolyte interface, where the interfacial microenvironment plays a pivotal role.[23,24] In particular, the interfacial hydrophobicity is

Received: February 24, 2025
Revised: April 1, 2025
Accepted: April 2, 2025
Published: April 10, 2025

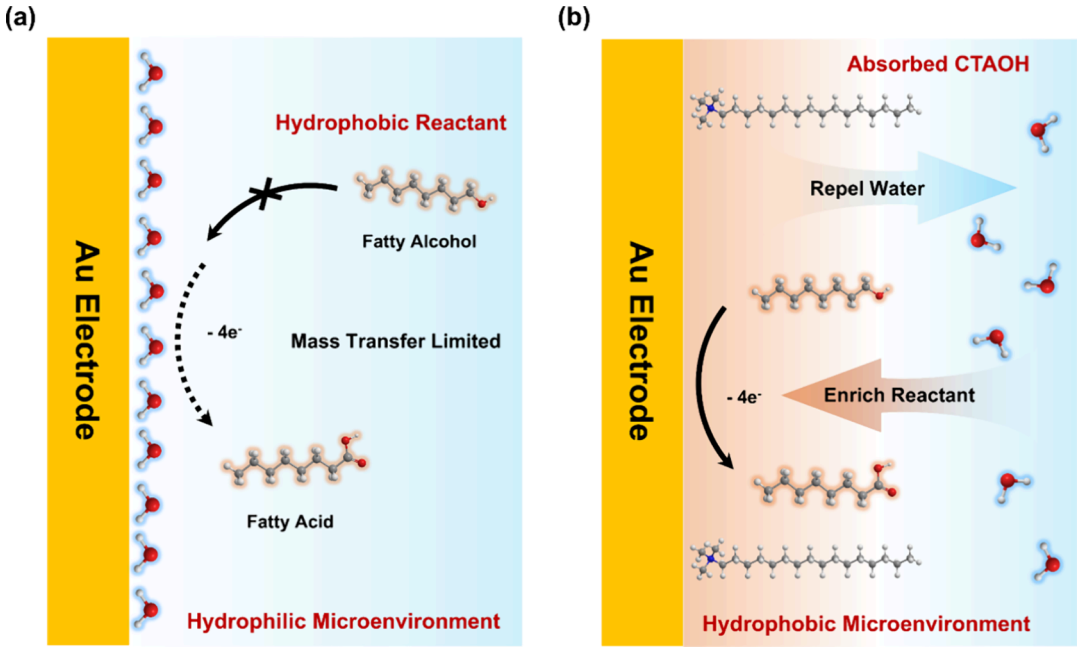

Figure 1. Schematic illustration of (a) the challenges associated with the electrocatalytic oxidation of fatty alcohols and (b) the electrolyte engineering strategy proposed in this study to address these challenges.

a key factor that shapes both activity and selectivity in many electrocatalytic reactions.[25,26] The incorporation of electrolyte additives is considered effective in enhancing interfacial hydrophobicity, thus improving reactant accessibility to the electrode.[27,28] For instance, in the industrial electrosynthesis of adiponitrile, which is challenged by the low aqueous solubility of acrylonitrile, the addition of quaternary ammonium salts promotes acrylonitrile accumulation near the electrode surface and mitigates competitive hydrogen evolution side reactions.[29] Despite these advancements, research focusing on enhancing mass transfer through the modulation of interfacial hydrophobicity in organic electrocatalytic oxidation remains in its early stages, with mechanistic insights still underexplored.

Herein, we introduce cetyltrimethylammonium hydroxide (CTAOH) as an electrolyte additive to modulate interfacial hydrophobicity, aiming to achieve efficient electrocatalytic fatty alcohol oxidation coupled with hydrogen production (Figure 1b). The addition of CTAOH significantly enhances the oxidation activity of fatty alcohols and the production rate of fatty acids on the Au electrocatalyst. Combining experimental and simulation results, we confirm that the preferential adsorption of CTAOH constructs a hydrophobic microenvironment at the electrode−electrolyte interface. This facilitates the enrichment of fatty alcohol reactants at the interface, thereby enhancing mass transfer performance. This work establishes electrolyte engineering as an effective strategy for boosting the electrocatalytic oxidation of fatty alcohols, which can be potentially extended to a broad spectrum of organic substrates with hydrophobic characteristics.

2. RESULTS AND DISCUSSION

Given the inherently hydrophobic nature of fatty alcohols, enhancing the interfacial hydrophobicity can improve the affinity of the electrode for these substrates. The amphiphilic surfactant CTAOH, which features a hydrophobic alkyl chain and a hydrophilic quaternary ammonium group, was employed as an electrolyte additive to modulate the interfacial hydrophobicity. To investigate the effect of CTAOH on the electrocatalytic oxidation of fatty alcohols, octanol was selected as a model substrate. As shown in Figure S1, the oxidation current density of octanol on Au foil increased significantly with higher CTAOH concentrations, indicating that CTAOH promotes the electro-oxidation of octanol. Notably, in the absence of octanol, CTAOH did not exhibit any oxidation activity on the Au foil (Figure S2), confirming that the observed enhancement can be attributed to the oxidation of fatty alcohols.

It is well known that surfactants such as CTAOH form micelles in bulk solution when their concentration exceeds the critical micelle concentration (CMC), thereby enhancing the solubility of hydrophobic organic compounds. To verify this, we measured the surface tension of the electrolyte as a function of the CTAOH concentration (Figure S3). The results confirm that micelle formation occurs at CTAOH concentrations above 0.2 mM. Gas chromatography further revealed that the introduction of 0.25 mM CTAOH more than doubled the octanol concentration in the bulk solution (Figure S4), demonstrating its solubilization effect. However, increasing the CTAOH concentration beyond this point did not significantly alter the octanol concentration.

To determine whether solubilization contributes to the observed activity enhancement, we compared linear sweep voltammetry (LSV) curves on Au foil in 1 M KOH with and without 10 mM CTAOH, both saturated with octanol (Figure S5). Surprisingly, despite the higher octanol concentration in the bulk solution with 10 mM CTAOH, the oxidation activity decreased. This indicates that micelles encapsulate octanol, limiting its access to the electrode surface,[30] and thus rules out bulk solubilization as the primary factor for the observed activity enhancement. Interestingly, we observed that as the amount of octanol added to the electrolyte with 10 mM CTAOH increased, the oxidation current density on the Au foil significantly improved (Figure S6). This indicates that the undissolved octanol primarily participates in the reaction and

https://doi.org/10.1021/jacsau.5c00215
JACS Au 2025, 5, 1974−1982

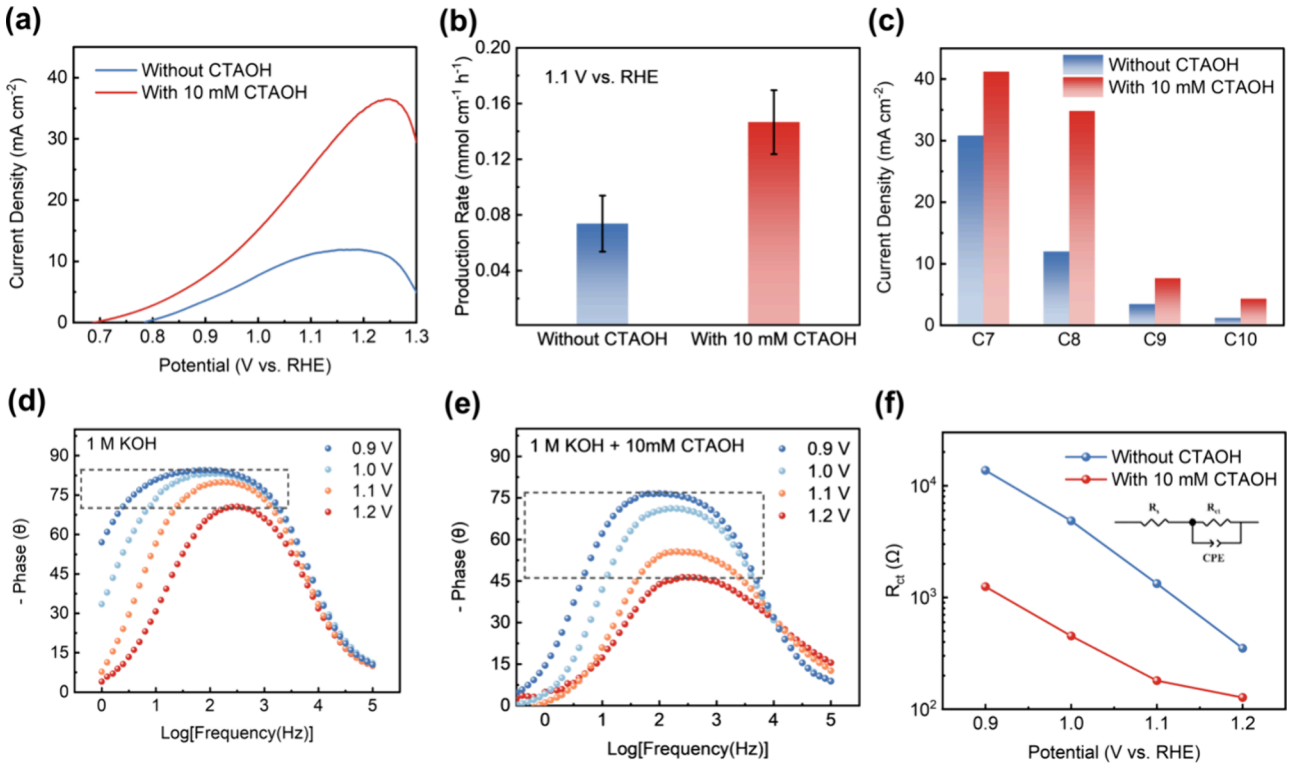

Figure 2. (a) LSV curves for the electrocatalytic oxidation of octanol in 1 M KOH with and without 10 mM CTAOH. (b) Production rate of octanoic acid on ED-Au/NF at 1.1 V vs RHE in 1 M KOH with and without the addition of 10 mM CTAOH. (c) Comparison of oxidation current density for fatty alcohol with different alkyl chain lengths at 1.2 V vs RHE on ED-Au/NF. (C7: heptanol, C8: octanol, C9: nonanol, C10: decanol). Bode plots of in situ EIS tests on ED-Au/NF in 1 M KOH (d) with and (e) without 10 mM CTAOH. (f) Charge transfer resistance with and without CTAOH measured at various potentials; the inset shows the equivalent circuit model for the fitting of the Nyquist plots. Unless otherwise specified, all reactions were conducted in 15 mL of 1 M KOH aqueous electrolyte with 1.5 mmol of the reactant at room temperature.

contributes to the enhanced activity induced by CTAOH. This finding prompts us to explore the role of CTAOH from the perspective of the interfacial microenvironment in subsequent investigations.

To enhance the specific surface area and activity, a gold electrocatalyst was deposited on nickel foam (NF) via galvanostatic electrodeposition, denoted as ED-Au/NF. Scanning electron microscopy (SEM) revealed a nanoflower-like morphology (Figure S7), indicative of a high specific surface area. Transmission electron microscopy (TEM) further revealed dendritic microstructures (Figure S8), with elemental analysis confirming the presence of gold. Since the electrodeposition process was conducted in an acidic solution, nickel from the NF substrate underwent dissolution and subsequent redeposition, inevitably resulting in trace amounts of nickel element. High-resolution TEM images (Figure S8d) exhibited lattice fringes corresponding to the (111) crystallographic plane of gold, with an interplanar spacing of 0.235 nm.[31] X-ray diffraction (XRD) spectra, illustrated in Figure S3a, affirm the polycrystalline nature of ED-Au/NF, with characteristic peaks at 38.2, 44.3, 64.6, and 77.5°, which are indexed to the gold phase (PDF# 04-0784), and additional peaks arising from the nickel substrate (PDF# 04-0850). High-resolution X-ray photoelectron spectroscopy (XPS) of the Au 4f region, as portrayed in Figure S3b, exhibits signature peaks at 83.5 and 87.1 eV, which are ascribed to metallic gold.[32] These findings collectively confirm the successful deposition of the gold electrocatalyst onto the NF substrate. Additionally, double-layer capacitance measurements demonstrated a significantly higher electrochemical active surface area (ECSA) for ED-Au/NF compared to that for Au foil (Figure S10).

As illustrated in Figure 2a, the introduction of CTAOH to 1 M KOH also significantly enhanced the electro-oxidation activity of octanol on ED-Au/NF. The peak current density increased remarkably from 12 to 40 mA cm^{-2}. According to previous studies,[33] the electrophilic OH* species on gold electrodes drive alcohol oxidation, while the formation of AuO_x at high potentials leads to passivation and a sharp decline in activity, explaining the peak-shaped LSV curves observed in Figure 2a. High-performance liquid chromatography (HPLC) was employed to analyze the fatty acid products generated during the constant potential electrolysis. As shown in Figure 2b, the incorporation of 10 mM CTAOH doubled the yield of octanoic acid at 1.1 V vs RHE. Moreover, ED-Au/NF exhibited remarkable stability over four cycles at 1.1 V vs RHE (Figures S11 and S12). Notably, the product analysis exclusively identified the octanoic acid signal peak, indicating 100% selectivity for octanoic acid during the electrocatalytic oxidation of octanol (Figure S13). This result underscores the potential of the electrocatalytic oxidation approach for fatty acid production, characterized by mild conditions and the absence of byproducts. Additionally, the phase separation of octanoic acid from the aqueous electrolyte upon acidification simplifies the product separation process (Figure S14).

Furthermore, the electrocatalytic oxidation of octanol, as an alternative to the oxygen evolution reaction, can substantially decrease the anodic potential (Figure S15), which is advantageous for reducing energy consumption for hydrogen production. Within a two-electrode configuration comprising

https://doi.org/10.1021/jacsau.5c00215
JACS Au 2025, 5, 1974−1982

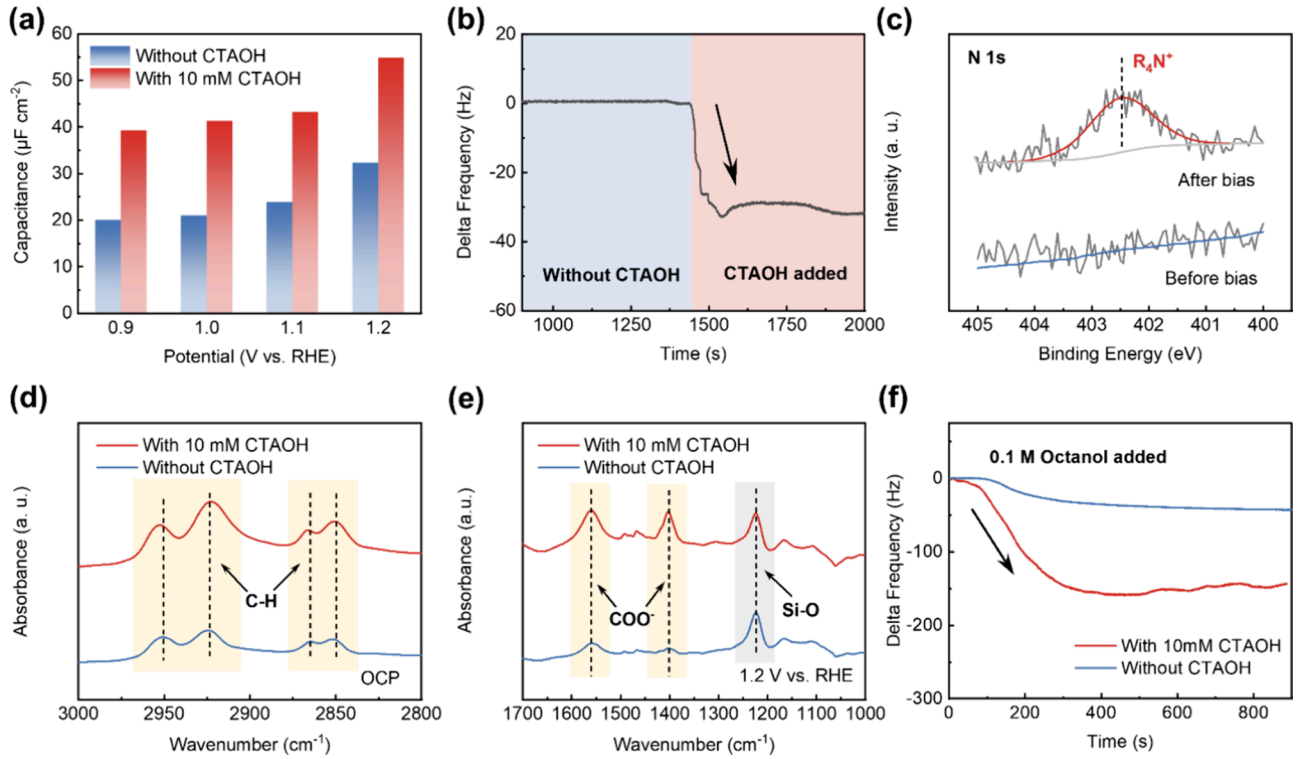

Figure 3. (a) Double-layer capacitance of Au foil measured at various potentials in 1 M KOH with and without 10 mM CTAOH. (b) QCM frequency response upon the addition of 10 mM CTAOH in 1 M KOH. (c) Ex-situ XPS spectra for the N 1s region of Au foil before and after anodic bias potential applied. (d) ATR-SEIRAS spectra in 1 M KOH and 1 M KOH with 10 mM CTAOH at OCP. (e) ATR-SEIRAS spectra in 1 M KOH and 1 M KOH with 10 mM CTAOH at 1.2 V vs RHE. (f) QCM frequency response upon the addition of octanol in 1 M KOH with and without 10 mM CTAOH.

ED-Au/NF and Pt foil, the introduction of octanol is found to reduce the cell voltage by 350 mV at 10 mA cm^{-2} (Figure S16). It is noteworthy that the presence of octanol or CTAOH does not exert any detrimental effects on the hydrogen evolution reaction (HER) activity on the Pt foil, as corroborated in Figure S17. The experimental hydrogen production volume at 10 mA cm^{-2} is found to closely match the theoretical prediction, confirming a Faradaic efficiency of 100% for the HER (Figure S18). Consequently, the integration of fatty alcohol electrocatalytic oxidation with hydrogen production emerges as a promising avenue for future applications.

Notably, the CTAOH-based electrolyte engineering strategy demonstrates a broad applicability to other fatty alcohols. As the carbon chain length increased, the oxidation activity of fatty alcohols on ED-Au/NF sharply decreased, which can be attributed to the reduced water solubility of longer-chain fatty alcohols (Figure S19). This result underscores the critical role of mass transfer performance in the electrocatalytic reaction of hydrophobic substrates such as fatty alcohols rather than the intrinsic activity of the catalyst. As shown in Figure 2c and Figure S20, the introduction of CTAOH enhanced the oxidation current density for heptanol (C7), nonanol (C9), and decanol (C10). These findings suggest that the electrolyte engineering strategy holds promise for extending to electrocatalytic oxidation processes of other hydrophobic organic substrates.

To further investigate interfacial behavior modulated by CTAOH, we employed in situ electrochemical impedance spectroscopy (EIS). We analyzed Bode and Nyquist plots in 1 M KOH with and without 10 mM CTAOH at potentials ranging from 0.9 to 1.2 V vs RHE. As shown in Figure 2d,e, with increasing potential, the phase angle peak shifted positively, indicating accelerated octanol electro-oxidation. Notably, the phase angle in 1 M KOH decreased only slightly from 83 to 70°, whereas in the presence of 10 mM CTAOH, it dropped significantly from 76 to 45°, reflecting enhanced electro-oxidation kinetics.[34,35] Additionally, charge transfer resistance (R_{ct}) was derived from the fitting of Nyquist plots at various potentials using an equivalent circuit model (Figure S21). Figure 2f shows a notable decrease in R_{ct} with the addition of 10 mM CTAOH, suggesting a faster charge transfer process in the electro-oxidation of octanol. To decipher the modulatory mechanisms of CTAOH on the electrode−electrolyte interface, we conducted a comparative analysis of the double-layer capacitance (C_{dl}) of Au foil with and without the presence of CTAOH. Cyclic voltammetry (CV) was utilized to ascertain the C_{dl} in proximity to the open-circuit potential (OCP), as delineated in Figure S22. The enhancement of C_{dl} from 30 to 55 $\mu F\ cm^{-2}$ upon the addition of CTAOH, as evidenced by the linear regression slope in Figure S22c, suggests a propensity for cetyltrimethylammonium cations (CTA^+) to adsorb at the interface, thereby augmenting the potential drop across the double layer. Moreover, the C_{dl} values at varied anodic potentials, as derived from the fitting results of in situ EIS, corroborate the higher C_{dl} of the CTAOH-containing system relative to the pure KOH system (Figure 3a), which is indicative of an accelerated interfacial charge transfer process.[34]

The adsorptive behavior of CTAOH was further scrutinized by using a quartz crystal microbalance (QCM). A notable reduction of approximately 30 Hz in the oscillation frequency

https://doi.org/10.1021/jacsau.5c00215
JACS Au 2025, 5, 1974−1982

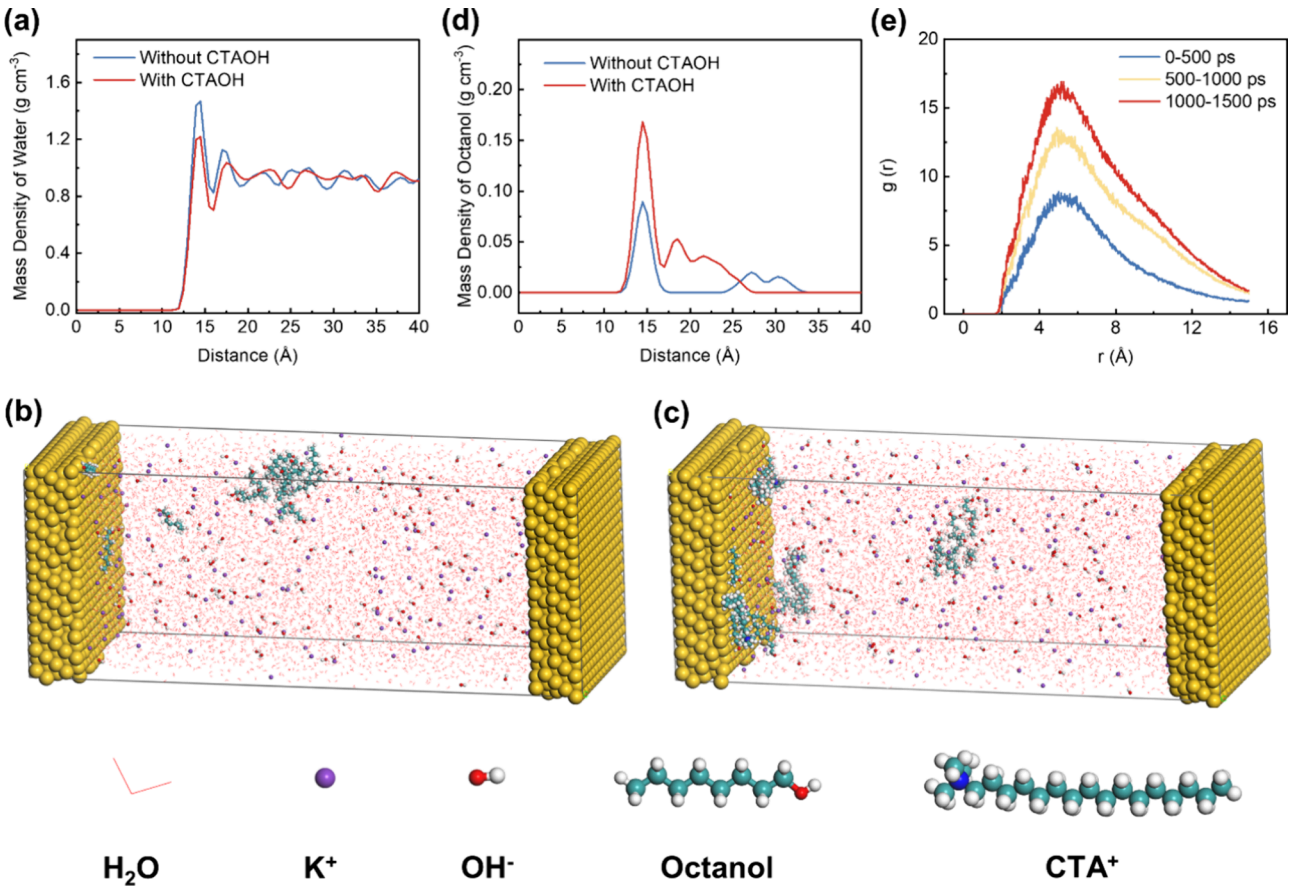

Figure 4. Snapshots of the final state for the (a) pure KOH system and the (b) CTAOH-containing system. (c) Density profiles of water calculated from MD simulations in the pure KOH system and CTAOH-containing system. (d) Density profiles of octanol calculated from MD simulations in pure KOH system and CTAOH-containing system. (e) Radial distribution functions of CTAOH-octanol obtained from MD simulations.

was observed when transitioning from a pure KOH solution to one containing CTAOH, as shown in Figure 3b. This change indicates the spontaneous adsorption of CTAOH at the OCP, resulting in an increase in the chip mass. Additionally, ex-situ X-ray photoelectron spectroscopy (XPS) spectra presented in Figure 3c reveal a nitrogen signal at 402.5 eV on the surface of the Au foil following the application of an anodic bias potential, corresponding to the R_4N^+ moiety found in CTAOH (Figure S23). Together, these results highlight the modulatory effect of CTAOH adsorption on the interfacial microenvironment.

Our subsequent investigation focuses on the influence of the hydrophobic interfacial microenvironment on the adsorption of fatty alcohols at the electrode interface. The variation in the OCP before and after the addition of organic reactants serves as an indicator of their adsorption within the inner Helmholtz layer.[36,37] As shown in Figure S24, following the addition of 0.1 M octanol, the OCP shift of the Au foil in 1 M KOH with 10 mM CTAOH was determined to be 50 mV, which is significantly greater than that observed in 1 M KOH alone (20 mV). This finding suggests that CTAOH facilitates the enrichment of octanol at the interface.

In situ attenuated total reflectance surface-enhanced infrared spectroscopy (ATR-SEIRAS), renowned for its heightened sensitivity to adsorbed species within the double layer, was employed to elucidate the impact of the interfacial microenvironment on the oxidation of octanol.[38] As depicted in Figure 3d, under the OCP, a quartet of peaks emerged in the wavenumber range of 2800−3000 cm^{-1}, corresponding to the stretching vibrations of the C−H bonds of the methyl and methylene groups within the octanol molecule.[7] Comparative analysis of these signal peak intensities indicates that CTAOH promotes the enrichment of octanol at the electrode−electrolyte interface. After a 5 min reaction at 1.2 V vs RHE, two distinct signal peaks could be observed at 1560 and 1403 cm^{-1} (Figure 3e). These peaks can be assigned to the antisymmetric and symmetric stretching vibrations of the carboxylate group ($-COO^-$) in potassium octanoate[39] (Figure S25). The CTAOH-containing system exhibited more pronounced signal peaks for the octanoic acid product, implying that the enrichment of octanol effectively enhanced its oxidation reaction rate.

QCM was utilized to quantitatively investigate the adsorption of octanol on the gold electrode surface. According to the Sauerbrey equation,[33] the frequency change is directly proportional to the mass change of the chip, thus allowing the calculation of the adsorptive mass of octanol, Δm, from the frequency change Δf before and after the addition of octanol. As illustrated in Figure 3f, the frequency change Δf in 1 M KOH with 10 mM CTAOH upon the addition of octanol was approximately 150 Hz, which is significantly higher than that in 1 M KOH (40 Hz). This indicates that the addition of CTAOH leads to a more than 2-fold increase in the adsorptive mass of octanol. In light of the experimental evidence presented, the introduction of CTAOH enhances the enrichment of octanol at the electrode−electrolyte interface, which is

https://doi.org/10.1021/jacsau.5c00215
JACS Au 2025, 5, 1974−1982

intrinsically linked to the hydrophobic microenvironment engineered by the adsorption of CTAOH.

Molecular dynamics (MD) simulations were conducted to gain a molecular-level understanding of how CTAOH influences the hydrophobicity of the electrode−electrolyte interface. The model consisted of a simulation box filled with 1 M KOH aqueous solution with Au (111) electrodes positioned at each end (for further details, refer to the Supporting Information). The spontaneous adsorption of CTA^+ onto the gold electrode surface, as observed in the simulation (Figure S26), was congruent with the experimental findings. For the pure KOH system, the local density of water molecules attained a maximum at the electrode−electrolyte interface, as portrayed in Figure 4a, indicative of the inherent hydrophilicity of the gold electrode. The introduction of CTAOH precipitated a marked reduction in the water molecule density in the interfacial vicinity. Consequently, we propose the mechanism by which CTAOH, as an electrolyte additive, modulates the interfacial microenvironment. In the absence of CTAOH, interfacial water enrichment at the electrode−electrolyte interface fosters a hydrophilic microenvironment. The spontaneous adsorption of CTA^+ onto the electrode surface, coupled with the hydrophobic effect exerted by the long alkyl chains of CTA^+, serves to repel the interfacial water, thereby establishing a hydrophobic interfacial microenvironment.[40,4140]

Further MD simulations were conducted to ascertain the diffusion behaviors of the octanol molecules. Figure S27 and S28 illustrate that a dozen octanol molecules are introduced into the simulation box, with their trajectories monitored over a duration of 2500 ps. Within a pure KOH system, octanol molecules, due to their hydrophobicity, tend to cluster in the solution bulk, with limited adsorption onto the electrode surface (Figure 4b). However, the presence of CTAOH facilitated the diffusion of these molecules toward the electrode, as portrayed in Figure 4c. The mass density distribution of octanol in the vicinity of the electrode, as presented in Figure 4d, indicates a higher local concentration of octanol in the CTAOH-containing system, relative to the pure KOH system. Additionally, the radial distribution function analysis, showcased in Figure 4e, delineated the dynamic migration of octanol toward CTAOH, underscoring the affinity between CTAOH and octanol. This observation substantiates that the hydrophobic interfacial microenvironment modulated by CTAOH promotes the migration of octanol toward the electrode.

In summary, mechanistic insights into the CTAOH-modulated electrode−electrolyte interface for boosting octanol electrocatalytic oxidation are hereby proposed. For the pure KOH system, the enrichment of interfacial water leads to a hydrophilic interfacial microenvironment, hindering the migration of octanol toward the electrode. The adsorption of CTAOH enhances the interfacial hydrophobicity, leading to the enrichment of octanol. Given the low solubility of octanol in water, the improvement in mass transfer performance can significantly enhance the electrocatalytic oxidation rate. Furthermore, since most organic compounds exhibit poor water solubility, the electrolyte engineering strategy proposed in this work has good versatility and scalability and is an effective approach to promote aqueous-phase electrocatalytic conversion of organic compounds.

3. CONCLUSIONS

In conclusion, this work developed an efficient electrocatalytic oxidation process for fatty alcohols, utilizing CTAOH as an electrolyte additive. The intrinsic low aqueous solubility of fatty alcohol, attributed to its long alkyl chains, poses a significant mass transfer challenge and limits the electro-oxidation rate on gold catalysts. Employing octanol as a model substrate, our findings demonstrate a marked enhancement in the electro-oxidation kinetics and a significant increase in the production yield of octanoic acid upon the introduction of CTAOH. Moreover, we demonstrate the feasibility of integrating the electrocatalytic oxidation of fatty alcohols with the HER at the cathode to diminish the energy demands of hydrogen production.

Our mechanistic investigations reveal that CTAOH preferentially adsorbs on the electrode surface, resulting in a reduction in interfacial water density and the formation of a hydrophobic interface. Utilizing a comprehensive approach that integrates QCM, in situ ATR-SEIRAS, and MD simulations, we have substantiated that the hydrophobic interface, modulated by CTAOH, facilitates the enrichment of octanol at the electrode−electrolyte interface, thereby enhancing its mass transfer efficiency. The strategy of modulating interfacial hydrophobicity through electrolyte engineering, as outlined in this work, holds promise for broader application in aqueous-phase electrocatalytic conversion processes involving water-insoluble organic substrates.

4. EXPERIMENTAL AND THEORETICAL METHODS

4.1. Material Characterization

SEM images were obtained by using a JEOL JSM-7900F scanning electron microscope. TEM images were acquired with a JEOL JEM-2010 transmission electron microscope. XPS spectra were recorded using an AXIS Supra+ instrument (Kratos, England), with the C 1s peak at 284.8 eV serving as a calibration reference for determining accurate binding energies. XRD patterns were collected using a Bruker D8 ADVANCE.

4.2. Electrode Preparation

Prior to usage, NF was thoroughly cleaned by rinsing with 3 M hydrochloric acid, ultrapure water, and ethanol. The electrodeposition of ED-Au/NF was performed at 0.5 mA cm^{-2} for 600 s in a solution of 10 mM $HauCl_4$ and 0.5 M H_2SO_4. The cleaned NF acted as the cathode, while a graphite plate was used as the anode. Following the electrodeposition, ED-Au/NF was rinsed sequentially with ultrapure water and ethanol and then dried at 40 °C.

4.3. Electrochemical Measurement

All electrochemical measurements were conducted using a CHI760E electrochemical workstation. LSV tests were performed in a three-electrode cell without *iR* compensation, employing a platinum foil as the counter electrode and an Hg/HgO reference electrode. Double-layer capacitances were determined by CV within a potential window of OCP ± 50 mV, with scan rates set at 10, 20, 30, 40, and 50 mV/s. The change in current density (Δj) was plotted against the scan rate, with the slope representing the estimated value of C_{dl}. EIS was conducted across a frequency range of 0.1 to 100,000 Hz at an amplitude of 5 mV, with measurements taken from 0.9 to 1.2 V vs RHE. The equivalent circuit shown in Figure 2i was employed to simulate experimental data points. Double-layer capacitances were calculated using established equations,[34] where C_{dl} denotes double-layer capacitance, R_{ct} indicates charge transfer resistance, CPE represents the constant phase element, and n is the fitting parameter determined from Nyquist plot analysis.

https://doi.org/10.1021/jacsau.5c00215
JACS Au 2025, 5, 1974−1982

$$\mathrm{Cdl} = \frac{(\mathrm{CPE} \times R_{ct})^{1/n}}{R_{ct}}$$

4.4. Product and Reactant Quantification

The quantification of octanol was performed using gas chromatography (GC, Shimadzu GC-2010) equipped with a flame ionization detector (FID). An AB-INOWAX column was used with nitrogen as the carrier gas. Product quantification was performed using HPLC (Shimadzu LC-20ADXR) equipped with a UV detector set to a wavelength of 210 nm. A Bio-Rad Aminex 87H column was utilized, and the eluent consisted of 5 mM aqueous H_2SO_4 mixed with 20% acetonitrile, at a flow rate of 0.6 mL min^{-1}. The faradaic efficiency for octanoic acid (OAc) was calculated using appropriate equations, with $n = 4$ representing the number of electrons transferred for OAc formation, and 96,485 C mol^{-1} as the Faraday constant.

$$\mathrm{OAc\ FE}(\%) = \frac{\text{mole of produced OAc} \times n \times 96485\ \mathrm{C\ mol^{-1}}}{\text{total charge passed}} \times 100\%$$

The generation of hydrogen was quantified by using a gas collection method in a two-electrode cell. The theoretical H_2 volume was calculated as follows, with 0.0244 mL mol^{-1} representing the molar volume of H_2 at 25 °C and 1 bar.

$$\text{theoretical } H_2 \text{ volume(mL)} = 0.0244\ \mathrm{mL\ mol^{-1}} \times \text{total charge passed}/(2 \times 96485\ \mathrm{C\ mol^{-1}})$$

4.5. In Situ Attenuated Total Reflection Surface-Enhanced Infrared Absorption Measurement

In situ ATR-SEIRAS measurements were conducted using a Thermo Fisher Nicolet is50 equipped with a mercury cadmium telluride (MCT) detector cooled with liquid nitrogen (Figure S29). A silicon prism, onto which a polycrystalline gold nanofilm was chemically deposited, served as the optical crystal. The gold catalyst was prepared on the silicon prism by using the previously described electrodeposition method and functioned as the working electrode. A platinum foil and Hg/HgO were used as the counter and reference electrodes, respectively. The spectral resolution was set to 4 cm^{-1}, with data collected at approximately 40 s per spectrum. Reference spectra for SEIRAS measurements were recorded at the OCP in a 1 M KOH electrolyte with and without 10 mM CTAOH.

4.6. Quartz Crystal Microbalance Test

QCM measurements were conducted in a flow cell using a QSense Explorer system (Biolin Scientific) at room temperature with gold-coated quartz sensors (Figure S30). The QCM test was initiated for approximately 300 s in 1 M KOH to reach steady state. Subsequently, a solution containing 10 mM CTAOH or 0.1 M octanol in 1 M KOH was introduced into the electrolyte and pumped into the QCM flow cell. The octanol-containing solution was stirred in advance to form an emulsion.

4.7. Molecular Dynamics Simulation

Molecular dynamics simulations were conducted using the Forcite module in the Materials Studio software, employing the COMPASS III force field for all simulations.[42] The simulation model consisted of Au (111) electrodes positioned at opposite ends of the simulation box with a separation of 12 nm between the inner surfaces of the electrodes. The region between the electrodes was filled with an electrolyte solution comprising 1 mol L^{-1} KOH and CTAOH molecules. Simulations were carried out in the NVT ensemble, with the system temperature maintained at 298 K. Long-range electrostatic interactions were calculated using the Ewald method, while van der Waals interactions were treated with the cutoff method, with a cutoff distance of 1.55 nm. The simulation time step was set to 1 fs, and each system underwent 1500 ps of MD simulation. Frame structures were recorded at intervals of 5 ps.

■ ASSOCIATED CONTENT

Supporting Information

The Supporting Information is available free of charge at https://pubs.acs.org/doi/10.1021/jacsau.5c00215.

Additional experimental and computational results, including catalyst characterization, product analysis, simulation snapshots, and photographs of the experimental setup (DOCX)

■ AUTHOR INFORMATION

Corresponding Authors

Haihui Wang − *Department of Chemical Engineering, Tsinghua University, Beijing 100084, P. R. China;* orcid.org/0000-0002-2917-4739; Email: cehhwang@tsinghua.edu.cn

Yi Cheng − *Department of Chemical Engineering, Tsinghua University, Beijing 100084, P. R. China;* orcid.org/0000-0002-0711-1884; Email: yicheng@tsinghua.edu.cn

Authors

Ruiqi Du − *Department of Chemical Engineering, Tsinghua University, Beijing 100084, P. R. China*

Zemao Chen − *Department of Chemical Engineering, Tsinghua University, Beijing 100084, P. R. China*

Shiyan Wang − *Department of Chemical Engineering, Tsinghua University, Beijing 100084, P. R. China*

Shumao Zeng − *Department of Chemical Engineering, Tsinghua University, Beijing 100084, P. R. China*

Rui Jia − *Department of Chemical Engineering, Tsinghua University, Beijing 100084, P. R. China*

Kaizheng Zhang − *Department of Chemical Engineering, Tsinghua University, Beijing 100084, P. R. China*

Diannan Lu − *Department of Chemical Engineering, Tsinghua University, Beijing 100084, P. R. China;* orcid.org/0000-0001-5993-5626

Complete contact information is available at: https://pubs.acs.org/10.1021/jacsau.5c00215

Notes

The authors declare no competing financial interest.

■ ACKNOWLEDGMENTS

Financial supports from the National Natural Science Foundation (No. 21991104 and No. 22278235) and International Joint Mission on Climate Change and Carbon Neutrality are acknowledged.

■ REFERENCES

(1) Najafishirtari, S.; Friedel Ortega, K.; Douthwaite, M.; Pattisson, S.; Hutchings, G. J.; Bondue, C. J.; Tschulik, K.; Waffel, D.; Peng, B.; Deitermann, M.; Busser, G. W.; Muhler, M.; Behrens, M. A Perspective on Heterogeneous Catalysts for the Selective Oxidation of Alcohols. *Chem. - Eur. J.* **2021**, *27* (68), 16809−16833.

(2) Anderson, R.; Griffin, K.; Johnston, P.; Alsters, P. L. Selective Oxidation of Alcohols to Carbonyl Compounds and Carboxylic Acids with Platinum Group Metal Catalysts. *Advanced Synthesis & Catalysis* **2003**, *345* (4), 517−523.

(3) Davis, S. E.; Ide, M. S.; Davis, R. J. Selective Oxidation of Alcohols and Aldehydes over Supported Metal Nanoparticles. *Green Chem.* **2013**, *15* (1), 17−45.
(4) Corberán, V. C.; González-Pérez, M. E.; Martínez-González, S.; Gómez-Avilés, A. Green Oxidation of Fatty Alcohols: Challenges and Opportunities. *Applied Catalysis A: General* **2014**, *474*, 211−223.
(5) Guo, L.; Liu, X.; Zhao, Z.; Lin, R.; Meng, Y.; Ma, X.; Li, Y.; Mou, X.; Yan, L.; Zhu, H.; Ding, Y. Nanostructured PtBi Alloy Enables Direct Oxidation of Linear α-Alcohols to Fatty Acids. *ACS Catal.* **2023**, *13* (19), 12571−12581.
(6) Su, Y.; Fan, R.; Li, J.; Liu, Y.; Zheng, Z.; Zhou, X.; Feng, X.; Liu, Y.; Zhao, H.; Chen, X.; Zhang, X.; Yang, C.; Yan, H. Interfacial Auδ−−OV−Ti Structure Promoted C−H Bond Activation for Selective Oxidation of Fatty Alcohols to Fatty Acids. *Ind. Eng. Chem. Res.* **2024**, *63* (30), 13115−13126.
(7) Yang, P.; Douthwaite, M.; Pan, J.; Zheng, L.; Hong, S.; Morgan, D. J.; Gao, M.; Li, D.; Feng, J.; Hutchings, G. J. Coordinately Unsaturated O2c−Ti5c−O2c Sites Promote the Reactivity of Pt/TiO2 Catalysts in the Solvent-Free Oxidation of n-Octanol. *Catal. Sci. Technol.* **2021**, *11* (14), 4898−4910.
(8) Mudugamuwa, C. J.; Xie, Y.; Zhang, K.; Nicholls, T. P.; Chalker, J. M.; Jia, Z. Nitroxide Radical Surfactants Enable Electrocatalytic Oxidation of Fatty Alcohols in Water. *Green Chem.* **2023**, *25* (8), 3086−3094.
(9) Ishida, T.; Ogihara, Y.; Ohashi, H.; Akita, T.; Honma, T.; Oji, H.; Haruta, M. Base-Free Direct Oxidation of 1-Octanol to Octanoic Acid and Its Octyl Ester over Supported Gold Catalysts. *ChemSusChem* **2012**, *5* (11), 2243−2248.
(10) Parmeggiani, C.; Cardona, F. Transition Metal Based Catalysts in the Aerobic Oxidation of Alcohols. *Green Chem.* **2012**, *14* (3), 547−564.
(11) Brink, G. J. t.; Arends, I. W. C. E.; Sheldon, R. A. Green, Catalytic Oxidation of Alcohols in Water. *Science* **2000**, *287* (5458), 1636−1639.
(12) Zhao, G.; Yang, F.; Chen, Z.; Liu, Q.; Ji, Y.; Zhang, Y.; Niu, Z.; Mao, J.; Bao, X.; Hu, P.; Li, Y. Metal/Oxide Interfacial Effects on the Selective Oxidation of Primary Alcohols. *Nat. Commun.* **2017**, *8* (1), 14039.
(13) Tang, D.; Lu, G.; Shen, Z.; Hu, Y.; Yao, L.; Li, B.; Zhao, G.; Peng, B.; Huang, X. A Review on Photo-, Electro- and Photoelectro-Catalytic Strategies for Selective Oxidation of Alcohols. *Journal of Energy Chemistry* **2023**, *77*, 80−118.
(14) Bender, M. T.; Yuan, X.; Choi, K.-S. Alcohol Oxidation as Alternative Anode Reactions Paired with (Photo)Electrochemical Fuel Production Reactions. *Nat. Commun.* **2020**, *11* (1), 4594.
(15) Zhou, D.; Tian, C.; Huang, H.; Zhu, W.; Luo, L.; Sun, X. Renewable Electricity Powered Chemical Industry at Anode: Opportunities. *Development and Perspectives. Nano Energy* **2024**, *128*, No. 109884.
(16) Prabhu, P.; Wan, Y.; Lee, J.-M. Electrochemical Conversion of Biomass Derived Products into High-Value Chemicals. *Matter* **2020**, *3* (4), 1162−1177.
(17) Li, Y.; Wei, X.; Chen, L.; Shi, J. Electrocatalytic Hydrogen Production Trilogy. *Angew. Chem., Int. Ed.* **2021**, *60* (36), 19550−19571.
(18) Luo, H.; Barrio, J.; Sunny, N.; Li, A.; Steier, L.; Shah, N.; Stephens, I. E. L.; Titirici, M.-M. Progress and Perspectives in Photo- and Electrochemical-Oxidation of Biomass for Sustainable Chemicals and Hydrogen Production. *Adv. Energy Mater.* **2021**, *11* (43), 2101180.
(19) Ureta-Zañartu, M. S.; Mascayano, C.; Gutiérrez, C. On the Dramatic Increase with Chain Length of the Oxidazability of Linear Saturated Aliphatic Alcohols on Gold in Alkaline Media. *Electrochim. Acta* **2015**, *165*, 232−238.
(20) Li, Z.; Li, X.; Zhou, H.; Xu, Y.; Xu, S.-M.; Ren, Y.; Yan, Y.; Yang, J.; Ji, K.; Li, L.; Xu, M.; Shao, M.; Kong, X.; Sun, X.; Duan, H. Electrocatalytic Synthesis of Adipic Acid Coupled with H2 Production Enhanced by a Ligand Modification Strategy. *Nat. Commun.* **2022**, *13* (1), 1−12.
(21) Ghosh, S.; Bagchi, D.; Mondal, I.; Sontheimer, T.; Jagadeesh, R. V.; Menezes, P. W. Deciphering the Role of Nickel in Electrochemical Organic Oxidation Reactions. *Adv. Energy Mater.* **2024**, *14* (22), 2400696.
(22) Bednarz, R. J.-R.; Jiménez-Meneses, P.; Gold, A. S.; Monllor-Satoca, D.; Stenglein, A.; Gómez, R.; Waldvogel, S. R. Sustainably Scaled Electrochemical Synthesis of 3-Propyladipic Acid in Line with Fluctuating Grid Supply. *ChemCatChem.* **2023**, *15* (17), No. e202300606.
(23) Sharifi Golru, S.; May, A. S.; Biddinger, E. J. Modifying Copper Local Environment with Electrolyte Additives to Alter CO2 Electroreduction vs Hydrogen Evolution. *ACS Catal.* **2023**, *13* (12), 7831−7843.
(24) Liu, Y.; Yang, Z.; Zou, Y.; Wang, S.; He, J. Interfacial Micro-Environment of Electrocatalysis and Its Applications for Organic Electro-Oxidation Reaction. *Small* **2024**, *20* (4), 2306488.
(25) Ji, K.; Liu, Y.; Wang, Y.; Kong, K.; Li, J.; Liu, X.; Duan, H. Steering Selectivity in Electrocatalytic Furfural Reduction via Electrode−Electrolyte Interface Modification. *J. Am. Chem. Soc.* **2024**, *146*, 11876.
(26) Zhong, Y.; Xu, Y.; Ma, J.; Wang, C.; Sheng, S.; Cheng, C.; Li, M.; Han, L.; Zhou, L.; Cai, Z.; Kuang, Y.; Liang, Z.; Sun, X. An Artificial Electrode/Electrolyte Interface for CO2 Electroreduction by Cation Surfactant Self-Assembly. *Angew. Chem.* **2020**, *132* (43), 19257−19263.
(27) Zhang, W.; Ge, W.; Qi, Y.; Sheng, X.; Jiang, H.; Li, C. Surfactant Directionally Assembled at the Electrode-Electrolyte Interface for Facilitating Electrocatalytic Aldehyde Hydrogenation. *Angew. Chem., Int. Ed.* **2024**, *63* (31), No. e202407121.
(28) Banerjee, S.; Gerke, C. S.; Thoi, V. S. Guiding CO2RR Selectivity by Compositional Tuning in the Electrochemical Double Layer. *Acc. Chem. Res.* **2022**, *55* (4), 504−515.
(29) Blanco, D. E.; Lee, B.; Modestino, M. A. Optimizing Organic Electrosynthesis through Controlled Voltage Dosing and Artificial Intelligence. *Proc. Natl. Acad. Sci. U.S.A.* **2019**, *116* (36), 17683−17689.
(30) Jiang, M.; Tan, J.; Chen, Y.; Zhang, W.; Chen, P.; Tang, Y.; Gao, Q. Promoted Electrocatalytic Hydrogenation of Furfural in a Bi-Phasic System. *Chem. Commun.* **2023**, *59* (21), 3103−3106.
(31) Zhang, W.; Wang, T.; Liu, C.; Duan, C.; Xiong, W.; Li, H. Hydrothermal Self-Assembly of Gold Nanoparticles Embed on Carbon Felt for Effective Nitrogen Reduction. *Advanced Energy and Sustainability Research* **2023**, *4* (11), 2300056.
(32) Fu, G.; Kang, X.; Zhang, Y.; Guo, Y.; Li, Z.; Liu, J.; Wang, L.; Zhang, J.; Fu, X.-Z.; Luo, J.-L. Capturing Critical Gem-Diol Intermediates and Hydride Transfer for Anodic Hydrogen Production from 5-Hydroxymethylfurfural. *Nat. Commun.* **2023**, *14* (1), 8395.
(33) Li, Z.; Yan, Y.; Xu, S.-M.; Zhou, H.; Xu, M.; Ma, L.; Shao, M.; Kong, X.; Wang, B.; Zheng, L.; Duan, H. Alcohols Electrooxidation Coupled with H2 Production at High Current Densities Promoted by a Cooperative Catalyst. *Nat. Commun.* **2022**, *13* (1), 147.
(34) Ge, W.; Chen, Y.; Fan, Y.; Zhu, Y.; Liu, H.; Song, L.; Liu, Z.; Lian, C.; Jiang, H.; Li, C. Dynamically Formed Surfactant Assembly at the Electrified Electrode−Electrolyte Interface Boosting CO2 Electroreduction. *J. Am. Chem. Soc.* **2022**, *144* (14), 6613−6622.
(35) Liu, Y.; Wang, L.; Zhang, Y.; Xie, J.; Li, J.; Wei, J.; Zhang, M.; Yang, Y. From Ethylene Glycol to Glycolic Acid: Electrocatalytic Conversion on Pt-Group Metal Surfaces. *Inorg. Chem.* **2024**, *63*, 14794.
(36) Heidary, N.; Kornienko, N. Electrochemical Biomass Valorization on Gold-Metal Oxide Nanoscale Heterojunctions Enables Investigation of Both Catalyst and Reaction Dynamics with Operando Surface-Enhanced Raman Spectroscopy. *Chem. Sci.* **2020**, *11* (7), 1798−1806.
(37) Du, M.; Zhang, Y.; Kang, S.; Xu, C.; Ma, Y.; Cai, L.; Zhu, Y.; Chai, Y.; Qiu, B. Electrochemical Production of Glycolate Fuelled By Polyethylene Terephthalate Plastics with Improved Techno-Economics. *Small* **2023**, *19* (39), 2303693.

https://doi.org/10.1021/jacsau.5c00215
JACS Au 2025, 5, 1974−1982

(38) Qi, Y.; Zhang, Y.; Yang, L.; Zhao, Y.; Zhu, Y.; Jiang, H.; Li, C. Insights into the Activity of Nickel Boride/Nickel Heterostructures for Efficient Methanol Electrooxidation. *Nat. Commun.* **2022**, *13* (1), 4602.
(39) Filopoulou, A.; Vlachou, S.; Boyatzis, S. C. Fatty Acids and Their Metal Salts: A Review of Their Infrared Spectra in Light of Their Presence in Cultural Heritage. *Molecules* **2021**, *26* (19), 6005.
(40) Zhao, Y.; Xu, J.; Huang, K.; Ge, W.; Liu, Z.; Lian, C.; Liu, H.; Jiang, H.; Li, C. Dopant- and Surfactant-Tuned Electrode−Electrolyte Interface Enabling Efficient Alkynol Semi-Hydrogenation. *J. Am. Chem. Soc.* **2023**, *145* (11), 6516−6525.
(41) Dorchies, F.; Serva, A.; Crevel, D.; De Freitas, J.; Kostopoulos, N.; Robert, M.; Sel, O.; Salanne, M.; Grimaud, A. Controlling the Hydrophilicity of the Electrochemical Interface to Modulate the Oxygen-Atom Transfer in Electrocatalytic Epoxidation Reactions. *J. Am. Chem. Soc.* **2022**, *144* (49), 22734−22746.
(42) Sharma, S. *Molecular Dynamics Simulation of Nanocomposites Using BIOVIA Materials Studio, Lammps and Gromacs*; Elsevier, 2019.

https://doi.org/10.1021/jacsau.5c00215
JACS Au 2025, 5, 1974−1982